

Geophysical evidence from the MELT area for compositional controls on oceanic plates

Q1

Rob. L. Evans¹, Greg Hirth¹, Kiyoshi Baba³, Don Forsyth⁴, Alan Chave² & Randall Mackie⁵

Magnetotelluric and seismic data, collected during the MELT experiment at the southern East Pacific Rise^{1,2}, constrain the distribution of melt beneath this mid-ocean-ridge spreading centre and also the evolution of the oceanic lithosphere during its early cooling history. Here we focus on structures imaged at distances ~ 100 to 350 km east of the ridge crest, corresponding to seafloor ages of ~ 1.3 to 4.5 million years (Myr), where the seismic and electrical conductivity structure is nearly constant and independent of age. Beginning at a depth of about 60 km, we image a large increase in electrical conductivity and a change from isotropic to transversely anisotropic electrical structure, with higher conductivity in the direction of fast propagation for seismic waves. Conductive cooling models predict structure that increases in depth with age, extending to about 30 km at 4.5 Myr ago. We infer, however, that the structure of young oceanic plates is instead controlled by a decrease in water content above a depth of 60 km induced by the melting process beneath the spreading centre³.

MELT magnetotelluric response functions were inverted for a transversely anisotropic conductivity structure, described by three distinct conductivities in the ridge-parallel (x), ridge-perpendicular (y) and vertical (z) directions. Anisotropy oriented oblique to the ridge was not considered because shear-wave splitting demonstrates that the horizontal symmetry axis for seismic anisotropy is oriented approximately perpendicular to the ridge in the direction of seafloor spreading⁴. The inversion algorithm finds optimally smooth sets of models that fit the data to a desired level of misfit⁵. The degree of anisotropy permitted by the inversion is controlled by a regularization parameter (α) that restricts the level of closeness between the final models in the x , y and z directions. Setting α to 0 allows a freely anisotropic model, while increasing α forces the models in all three directions to be increasingly similar, resulting in an isotropic solution when α is large. All models account primarily for two-dimensional heterogeneity in resistivity structure and anisotropy is only included where needed to decrease misfit further. As expected, the model misfit decreases with decreasing α . Magnetotelluric data are generally not sensitive to the vertical conductivity, except where there are strong, vertical conduction pathways to the surface. Such links do not exist off-axis and so the vertical conductivity structure is not independently resolved. The full results of these inversions are given elsewhere⁶.

Inversions of the magnetotelluric response functions find higher conductivity in the direction of plate spreading with the transition from an electrically isotropic, resistive layer in the shallow upper mantle to an anisotropic conductive region beginning at a depth of around 60 km (Fig. 1). Mantle conductivity is influenced by temperature, composition—including volatile components—and the presence of partial melt. The relatively constant depth of the

resistive-to-conductive boundary at around 60 km indicates that the cause for the change in conductivity is not thermal. This depth is significantly greater than that predicted by models of conductive cooling for the age of the lithosphere in this region. For example, using a standard cooling model⁷ and a potential temperature of 1,350 °C, the depth to the 1,250 °C isotherm increases from only 17 to 29 km between 1.3 and 4.5 Myr ago.

Inversions of Rayleigh- and Love-wave data from the same area also find structure that is nearly independent of age. After a rapid increase in shear velocity to a depth of about 60 km beneath young sea floor within 100 km of the spreading centre, the velocity contours to the east of the ridge are nearly horizontal^{8,9}, decreasing from about 4.5 km s⁻¹ immediately beneath the Mohorovic discontinuity (Moho) to a minimum of about 4.1 km s⁻¹ at about 70 km

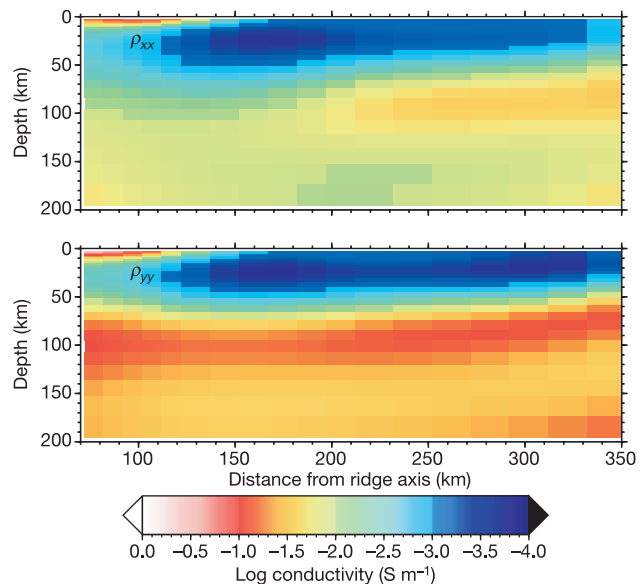


Figure 1 | Two model cross-sections of conductivity through the region 70–350 km east of the southern East Pacific Rise in the MELT area. The two sections show conductivity in the ridge-parallel (x) direction (top) and plate spreading (y) direction (bottom). The model was obtained using an anisotropic regularization parameter, $\alpha = 0.1$, in the inversion. The key features in the model are the resistive layer above about 60 km depth and the underlying conductive region that extends to about 120 km depth. The high-conductivity region is more conductive in the direction of plate spreading, which is also expected to be the direction of dominant a -axis olivine alignment.

¹Department of Geology and Geophysics, Woods Hole Oceanographic Institution, ²Department of Applied Ocean Physics and Engineering, Woods Hole Oceanographic Institution, Woods Hole, Massachusetts 02543, USA. ³Institute for Research on Earth Evolution, Japan Agency for Marine-Earth Science and Technology, 2-15, Natsushima, Yokosuka, Kanagawa, 237-0061, Japan. ⁴Department of Geology, Brown University, USA. ⁵GSY-USA, Inc., PMB#643, 2261 Market Street, San Francisco, California 94114, USA.

(Fig. 2). Here we emphasize structure to the east of the ridge, because the sea floor to the west subsides anomalously slowly, is populated by an unusual density of seamounts, and is poorly constrained by the magnetotelluric coverage. Unlike the conductivity structure, the shear structure in the uppermost 60 km of the mantle is required by the Rayleigh-wave data to be azimuthally anisotropic^{10–12}, with a fast direction perpendicular to the ridge consistent with the fast polarization direction observed from shear-wave splitting analyses⁴. (A discussion of whether electrical anisotropy can be resolved above 60 km is included in the Supplementary Information.) In addition, the magnitude of shear-wave splitting suggests that the anisotropic layer extends much deeper than 60 km.

To compare the results of our inversions to laboratory constraints on the conductivity of mantle minerals we calculated laterally averaged log-conductivity depth profiles from our models for both the plate-spreading (y) and ridge-parallel (x) directions. Examples are shown in Fig. 3 for models with $\alpha = 0.1$ (moderately anisotropic) and $\alpha = 10$ (effectively isotropic). Regardless of the degree of anisotropy in the inversions, a persistent feature is a large region of high conductivity east of the ridge. For the anisotropic models—that is, with $\alpha < 10$ —the conductivity parallel to the spreading direction is always greater than that parallel to the ridge axis. The anisotropy in conductivity is greatest from depths of ~ 70 to 150 km.

In the isotropic model (Fig. 3a) the conductivity at depths greater than ~ 100 km is significantly greater than that predicted from laboratory data for dry peridotite at a potential temperature of $1,350^\circ\text{C}$. The laboratory-based conductivity profiles are calculated using a temperature profile for 3-Myr-old lithosphere, assuming a mantle comprised of 75% olivine and 25% orthopyroxene¹³. There is almost no error associated with extrapolation of the experimental data because the measurements were made at the conditions of interest. However, the laboratory data¹⁴ exhibit a sample-to-sample variability of the order of a factor of two in conductivity. While the conductivity at depths greater than 100 km could be explained by a potential temperature of $\sim 1,500^\circ\text{C}$, this value is considerably greater than typically predicted for the upper mantle beneath the southern East Pacific Rise.

At depths greater than 100 km, the laterally averaged conductivity parallel to the spreading direction in our anisotropic model is similar to that predicted by the Nernst–Einstein relation for hydrogen diffusion parallel to the [100] direction in olivine containing $10^3\text{ H}/10^6\text{ Si}$ (Fig. 3b)¹⁵. We emphasize that the plots in Fig. 3 are calculated using hydrogen self-diffusivities¹⁶, which is appropriate for application of the Nernst–Einstein relation. The hydrogen self-diffusivity is estimated from the analysis of hydrogen chemical diffusion data^{16,17}. Even including the uncertainties in the hydrogen diffusion data, calculated conductivities predicted for the other

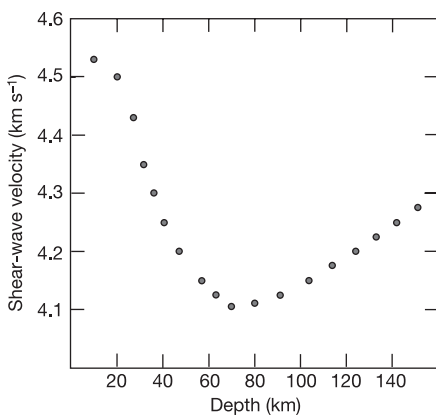


Figure 2 | Shear-wave velocity profile obtained through inversion of Rayleigh-wave data in the same region as Fig. 1.

crystallographic directions are significantly smaller (Fig. 3c). Therefore, anisotropy in conductivity is possible if there is a strong lattice preferred orientation of olivine in the peridotite imposed by corner flow. The factor-of-four anisotropy predicted for the laterally averaged model in Figs 3b and c is the same as that calculated for peridotite with $\sim 50\%$ alignment of the olivine [100] axes¹⁸, a value consistent with the 3%–5% azimuthal anisotropy of Rayleigh waves observed in this region.

An important caveat to the application of the hydrogen diffusion data to constrain mantle conductivity is that the influence of hydrogen on conductivity of olivine has not been measured experimentally, although it has been observed for wadsleyite and ringwoodite¹⁹. A critical factor to be determined is the fraction of hydrogen that contributes to the conductivity^{17,19}. In our calculations we have assumed that all of the hydrogen is contributing, and thus we predict a maximum influence of hydrogen on conductivity.

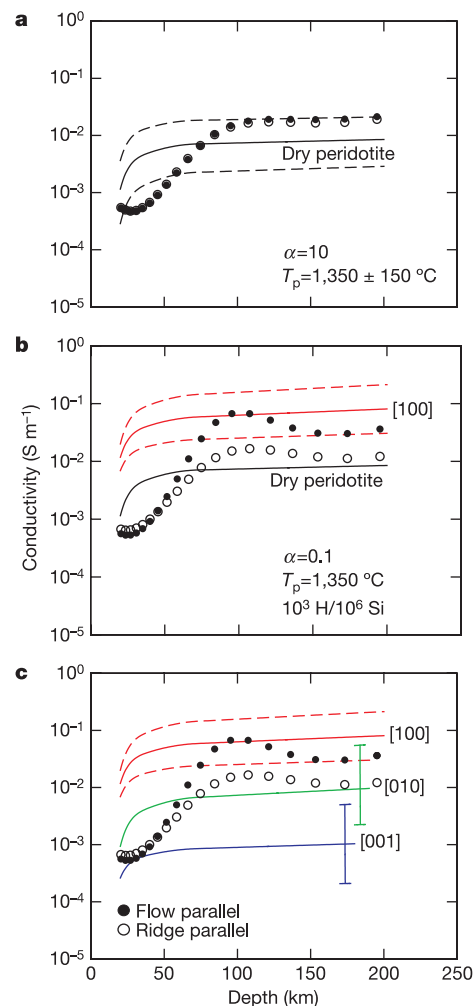


Figure 3 | Average one-dimensional profiles through our conductivity model and theoretical curves based on laboratory data. Comparisons between averaged values of conductivity from the MELT area with laboratory data on mantle conductivity. **a**, An isotropic model compared to conductivity of a dry peridotite mantle on a 3-Myr-old geotherm and an adiabat with a potential temperature of $T_p = 1,350^\circ\text{C}$. The upper and lower errors (dashed lines) show the effects of a variation in adiabat temperature of 150°C . **b**, Average conductivities through an anisotropic model compared to the predicted conductivity along the a axis of olivine shown with estimates of experimental errors. **c**, Same as **b** but with the conductivities in the three crystallographic directions shown as labelled. We used an olivine hydrogen content of $10^3\text{ H}/10^6\text{ Si}^3$ and hydrogen diffusion data¹⁶ to calculate conductivity using the Nernst–Einstein relation.

Because dissolved hydrogen influences the concentration of other defects within olivine, conductivity could also be enhanced under hydrous conditions by an increase in the concentration of metal vacancies. However, analyses based on the measured effect of water on Mg–Fe interdiffusion in olivine suggest that this effect is not large enough to explain the high conductivities observed in the oceanic mantle²⁰.

Two key sets of observations lead us to conclude that the mantle above 60 km is dehydrated, but significant dissolved hydrogen is present at greater depths. First, although the oceanic mantle is seismically anisotropic from the Moho to depths exceeding 100 km, significant electrical anisotropy and high conductivities are only resolved at depths exceeding 60 km. If the lattice preferred orientation does not change, the simplest explanation is that the higher anisotropic conductivities are caused by the anisotropic diffusivity of hydrogen. The orientation of the high-conductivity direction coincides with the fast direction for seismic wave propagation, as is expected if both are controlled by the lattice preferred orientation of olivine crystals in a deforming mantle. Second, if thermal effects were dominant, both the shear velocity and resistivity should gradually increase with increasing age and the high-resistivity, high-velocity region should be limited to much shallower depths.

The minimum in shear velocity observed at the same depth as at the start of the increase in conductivity can be caused either by the presence of melt, water (that is, dissolved hydrogen) or a combination of both. Melt affects velocity through elastic and anelastic effects^{21–23}, whereas dissolved water primarily affects velocities through anelastic effects^{24,25}. Therefore, using seismic data to discriminate between the presence of melt and water will require determination of the attenuation structure beneath this region of the mantle. Under the damp conditions we are inferring for the mantle below 60 km, the mantle would be above the solidus, allowing a small amount of melt to be present. The magnetotelluric and seismic data are most consistent with a small melt fraction (<2%) in a hydrous environment at depths greater than 60 km, with a maximum melt concentration at about 70 km. At shallower depths, increased melting and melt migration beneath the ridge axis would extract the water from the mantle minerals and the melt is expected to be removed to form the oceanic crust. The water content remaining in the mantle minerals would be significantly reduced in any residual mantle carried off-axis that had reached melt fractions greater than ~0.5% (refs 3, 26).

An alternative explanation for the abrupt increase in conductivity below 60 km is that the conductivity is controlled by melt below this boundary. In this case the change in physical properties would still represent a compositional boundary because melting at these conditions requires the presence of volatiles. If melt is the explanation for the conductivity enhancement, then the 60-km transition must act as an impermeable boundary, impeding the melt from rising. However, to account for the anisotropic conductivity, the melt would need to be distributed in tubes parallel to the spreading direction—and there is no known mechanism that would cause the melt to reside in such tubes. In addition, the abrupt change from resistive to conductive structure at approximately 60 km is also observed directly beneath the ridge axis where melting is ongoing at depths shallower than 60 km (ref. 6). The observation that conductivity remains significantly greater than that for dry olivine at depths up to ~200 km in the Pacific mantle²⁷ argues for a solid-state conduction mechanism involving dissolved water, because melting at depths greater than about 80 km requires the presence of water, melting at depths greater than about 125 km is difficult even in damp conditions, and the shear-wave velocity increases at depths greater than 80 km, suggesting the progressive elimination of melt.

Melting beneath the ridge dehydrates only the uppermost 60 km of the mantle, consistent with petrological models that suggest there is a

only a very small degree of melting in the presence of water at greater depths, with higher degrees of melting beginning at about 60 km where the geotherm beneath the ridge axis exceeds the dry solidus. The resulting dry region of upper mantle will have a viscosity significantly greater than the underlying asthenosphere, creating a rheological boundary layer³ that is compositionally and not thermally controlled. Our observations are broadly consistent with seismic data from the central Pacific that show a discontinuity (G) at a depth of 68 km, corresponding to the same dry–wet transition²⁸. This boundary corresponds to the base of the layer of low electrical conductivity and high shear-wave velocity observed in the MELT area.

Received 9 March; accepted 29 June 2005.

- MELT Seismic Team, Imaging the deep seismic structure beneath a mid-ocean ridge: the MELT experiment. *Science* **280**, 1215–1218 (1998).
- Evans, R. L. *et al.* Asymmetric electrical structure in the mantle beneath the East Pacific Rise at 17°S. *Science* **286**, 756–759 (1999).
- Hirth, G. & Kohlstedt, D. L. Water in the oceanic upper mantle: implications for rheology, melt extraction and the evolution of the lithosphere. *Earth Planet. Sci. Lett.* **144**, 93–108 (1996).
- Wolfe, C. J. & Solomon, S. C. Shear-wave splitting and implications for mantle flow beneath the MELT region of the East Pacific Rise. *Science* **280**, 1230–1232 (1998).
- Rodi, W. & Mackie, R. L. Nonlinear conjugate gradients algorithm for 2-D magnetotelluric inversion. *Geophysics* **66**, 174–187 (2001).
- Baba, K., Chave, A., Evans, R. L., Hirth, G. & Mackie, R. Mantle dynamics beneath the East Pacific Rise at 17°S: Insights from the MELT EM data. *J. Geophys. Res.* (submitted).
- Parsons, B. & Sclater, J. Variation of ocean floor bathymetry and heat flow with age. *J. Geophys. Res.* **82**, 803–827 (1977).
- Conder, J. A., Forsyth, D. W. & Parmentier, E. M. Asthenospheric flow and the asymmetry of the East Pacific Rise, MELT area. *J. Geophys. Res.* **107**(B12), 2344, doi:10.1029/2001JB000807 (2002).
- Dunn, R. A. & Forsyth, D. W. Imaging the transition between the region of mantle melt generation and the crustal magma chamber with short-period Love wave propagation along the southern East Pacific Rise. *J. Geophys. Res.* **108**(B7), 2352, doi:10.1029/2002JB002217 (2003).
- Nishimura, C. & Forsyth, D. W. The anisotropic structure of the upper mantle in the Pacific. *Geophys. J. R. Astron. Soc.* **96**, 203–229 (1989).
- Forsyth, D. W., Webb, S. C., Dorman, L. M. & Shen, Y. Phase velocities of Rayleigh waves in the MELT experiment on the East Pacific Rise. *Science* **280**, 1235–1238 (1998).
- Forsyth, D. W. & Li, A. Array-analysis of two-dimensional variations in surface wave velocity and azimuthal anisotropy in the presence of multipathing interference. In *Seismic Data Analysis and Imaging with Global and Local Arrays* (eds Levander, A. & Nolet, G.) (AGU Geophys. Monogr., in the press).
- Xu, Y. S., Shankland, T. J. & Poe, B. T. Laboratory-based electrical conductivity in the Earth's mantle. *J. Geophys. Res.* **105**, 27865–27875 (2000).
- Xu, Y. S., Shankland, T. J. & Duba, A. G. Pressure effect on electrical conductivity of mantle olivine. *Phys. Earth Planet. Inter.* **118**, 149–161 (2000).
- Karato, S. The role of hydrogen in the electrical conductivity of the upper mantle. *Nature* **347**, 272–273 (1990).
- Kohlstedt, D. L. & Mackwell, S. J. Diffusion of hydrogen and intrinsic point defects in olivine. *Z. Phys. Chem.* **207**, 147–162 (1998).
- Kohlstedt, D. & Mackwell, S. J. in *Microscopic Properties and Processes in Minerals* (eds Wright, K. & Catlow, R.) 539–559 (Kluwer Academic, Dordrecht, 1999).
- Simpson, F. Intensity and direction of lattice preferred orientation of olivine: are electrical and seismic anisotropies of the Australian mantle reconcilable? *Earth Planet. Sci. Lett.* **203**, 535–547 (2002).
- Huang, X., Xu, Y. & Karato, S. Water content in the transition zone from electrical conductivity of wadsleyite and ringwoodite. *Nature* **434**, 746–749 (2005).
- Hier-Mujander, S., Anderson, I. M. & Kohlstedt, D. L. Influence of protons on Fe–Mg interdiffusion in olivine. *J. Geophys. Res.* **110**, B02202, doi:10.1029/2004JB003292 (2005).
- Hammond, W. C. & Humphreys, E. D. Upper mantle seismic wave velocity: Effects of realistic partial melt geometries. *J. Geophys. Res.* **105**(B5), 10975–10986, doi:10.1029/2000JB900041 (2000).
- Hammond, W. C. & Humphreys, E. D. Upper mantle seismic wave attenuation: Effects of realistic partial melt distribution. *J. Geophys. Res.* **105**(B5), 10987–11000, doi:10.1029/2000JB900042 (2000).
- Faul, U. H., Fitz Gerald, J. D. & Jackson, I. Shear wave attenuation and dispersion in melt-bearing olivine polycrystals: 2. Microstructural interpretation and seismological implications. *J. Geophys. Res.* **109**, B06202, doi:10.1029/2003JB002407 (2004).
- Karato, S. Mapping water content in upper mantle. in *Inside the Subduction*

Q2

- Factory (ed. Eiler, J.) 135–152 (Geophys. Monogr. Ser. 138, American Geophysical Union, Washington DC, 2003).
25. Karato, S. Effects of water on seismic-wave velocities in the upper-mantle. *Proc. Jpn. Acad. Ser. B*, **71**, 61–66 (1995).
 26. Aubaud, C., Hauri, E. H. & Hirschmann, M. H. Water partition coefficients between nominally anhydrous minerals and basaltic melts. *Geophys. Res. Lett.* (in the press).
 27. Lizarralde, D., Chave, A. D., Hirth, G. & Schultz, A. Northeastern Pacific mantle conductivity profile from long-period magnetotelluric sounding using Hawaii-to-California submarine cable data. *J. Geophys. Res.* **100**, 17837–17854 (1995).
 28. Gaherty, J., Jordan, T. H. & Gee, L. S. Seismic structure of the upper mantle in a central Pacific corridor. *J. Geophys. Res.* **101**, 22291–22309 (1996).

Supplementary Information is linked to the online version of the paper at www.nature.com/nature.

Acknowledgements We thank S. Karato for comments. We are also grateful to S. Hier-Mujander and D. Kohlstedt for discussions. US participation in the MELT experiment and subsequent analysis was funded by NSF grants through the Marine Geology and Geophysics Program, Ocean Sciences Division.

Author Information Reprints and permissions information is available at npg.nature.com/reprintsandpermissions. The authors declare no competing financial interests. Correspondence and requests for materials should be addressed to R.L.E. (revans@whoi.edu).